NASA TECHNICAL NOTE

NASA TN D-7853

NASA TN D-7853

THE EFFECT OF RING DISTORTIONS ON BUCKLING OF BLUNT CONICAL SHELLS

by Walter L. Heard, Jr., Melvin S. Anderson, and Wendell B. Stephens

Langley Research Center
Hampton, Va. 23665

NATIONAL AERONAUTICS AND SPACE ADMINISTRATION • WASHINGTON, D. C. • FEBRUARY 1975

1. Report No.	2 Government Accession No.	3. Recipient's Catalog No.
NASA TN D-7853		

4 Title and Subtitle	5. Report Date
THE EFFECT OF RING DISTORTIONS ON BUCKLING OF BLUNT CONICAL SHELLS	February 1975
	6. Performing Organization Code

7 Author(s)	8. Performing Organization Report No.
Walter L. Heard, Jr., Melvin S. Anderson, and Wendell B. Stephens	L-9930
	10. Work Unit No. 505-02-51-01

9. Performing Organization Name and Address	11. Contract or Grant No.
NASA Langley Research Center Hampton, Va. 23665	
	13. Type of Report and Period Covered
12 Sponsoring Agency Name and Address	Technical Note
National Aeronautics and Space Administration Washington, D.C. 20546	14 Sponsoring Agency Code

15 Supplementary Notes

16. Abstract

A rigorous analytical study of cones stiffened by many thin-gage, open-section rings is presented. The results are compared with data previously obtained from uniform pressure tests of the Viking mission flight aeroshell and of the Viking structural prototype aeroshells. A conventional analysis, in which the rings are modeled as discrete rigid cross sections, is shown to lead to large, unconservative strength predictions. A more sophisticated technique of modeling the rings as shell branches leads to much more realistic strength predictions and more accurately predicts the failure modes. It is also shown that if a small initial imperfection proportional to the shape of the buckling mode is assumed, the critical buckling modes from analysis and test are in agreement. However, the reduction in buckling strength from the perfect-shell predictions is small.

17. Key Words (Suggested by Author(s))	18. Distribution Statement
Shell buckling Ring-stiffened shells Viking aeroshells	Unclassified – Unlimited STAR Category 32

19. Security Classif. (of this report)	20. Security Classif. (of this page)	21. No. of Pages	22. Price*
Unclassified	Unclassified	33	$3.75

*For sale by the National Technical Information Service, Springfield, Virginia 22151

THE EFFECT OF RING DISTORTIONS ON BUCKLING OF BLUNT CONICAL SHELLS

By Walter L. Heard, Jr., Melvin S. Anderson,
and Wendell B. Stephens
Langley Research Center

SUMMARY

A rigorous analytical study of the buckling strengths of large, blunt, conical shells stiffened by many thin-gage, open-section rings is presented. The results are compared with data previously obtained from uniform pressure tests of the Viking mission flight aeroshell (initial configuration) and of the Viking structural prototype aeroshells. The study shows that conventional analytical techniques, in which the small, thin-gage rings are modeled as discrete rigid cross sections, lead to large unconservative predictions of aeroshell buckling strengths. A more sophisticated technique of modeling the rings as portions of the shell structure (shell branches) leads to much more realistic predictions of buckling strengths and more accurately predicts the failure modes. It is also shown that if a small initial imperfection proportional to the shape of the buckling mode is assumed, the critical buckling modes from analysis and test are in agreement. However, the reduction in buckling strength from perfect-shell predictions is small.

INTRODUCTION

In the search for optimum designs of shell structures for space flight, the designer must consider thin-gage stiffened-construction concepts to meet the imposed low-mass requirements. In designing such structures, the engineer may be faced with possible failure modes amenable neither to classical stress and buckling formulas nor to well-established design procedures and structural modeling techniques. In reference 1, for example, it is shown that local deformations of stiffener cross sections may significantly reduce the shell strength; thus, shells with thin-gage stiffeners may require a rigorous analysis that can account for such deformations. Indeed, the application of conventional design practices can lead to unconservative strength predictions for highly optimized, lightly loaded, ring-stiffened shells which, typically, would be designed to approach all failure modes simultaneously. A prime example of the application of such a structure is the aerodynamic decelerator, or aeroshell, which will be used in the Project Viking

mission. (See ref. 2.) The aeroshell (see fig. 1) which is a ring-stiffened, blunt cone with a 3.5-meter base diameter will provide the initial deceleration of the payload prior to the parachute deployment in the Mars atmosphere. The structural prototype aeroshells and the first version of the actual flight aeroshell (see refs. 3 and 4) were optimally designed by using essentially identical design processes.

The design process used for the structural prototype aeroshell is described in detail in reference 4. The process was influenced strongly by the results of the buckling tests of two 4.6-meter base-diameter, magnesium, truncated cones stiffened with many small tubular rings and loaded under external pressure. (See ref. 5.) The results of reference 5 show that a general instability of the test specimens occurred at approximately 80 percent of the value predicted by theory (bifurcation buckling based on a linear stress state with the rings treated as discrete rigid cross sections). Thus the buckling behavior of both of these large stiffened cones was in agreement with previous results for isotropic cones. (The National Aeronautics and Space Administration design criteria manual (ref. 6) recommends that a knockdown factor of 0.75 on the general instability should provide a conservative, lower bound on buckling of unstiffened cones.) Based on this history, the use of a knockdown factor of 0.8 for the aeroshell design seemed entirely reasonable. The prototype aeroshell, however, was stiffened with many small rings with open cross sections (channels) in contrast to the closed-section, tubular rings of the previous stiffened-shell tests. The web width-to-thickness ratio of the rings located in the region of maximum buckling deflection was 33. Even though the shell did attain the design buckling-load goal because of other conservative assumptions, the comparison of test results with theory indicated that a 0.7 knockdown factor would have been more appropriate.

The flight aeroshell, although similar in gross dimension to the prototype, was fabricated from generally thinner gage material and was stiffened with many small Z-section rings with a web width-to-thickness ratio of 60. The shell also contained several reinforced cutouts. Because of these differences, and because of the data obtained from the prototype aeroshell tests, a 0.6 knockdown factor was used for design purposes. The design goal, however, was not attained for this shell in the initial buckling test, during which a general elastic buckling was observed at 75 percent of the minimum required capability.* The failure was attributed to ineffectiveness of the outstanding flanges of the Z-rings inasmuch as strain-gage output during loading indicated that these flanges remained stress free. Thus the very thin gage, open-section, stiffening rings may have become distorted in such a way that their stiffness was much less than that predicted by the classical ring theory.

*Test results and design details were supplied by H. E. Sparhawk, K. L. Fogg, and H. Brown of Martin Marietta Corporation.

As a result of these events and of recent advances that include branched-shell capability in shell-of-revolution analysis computer codes, a more detailed examination of the buckling behavior both of the prototype and of the flight aeroshells has been made by use of refined structural models. The purpose of this report is to show the effect of the ring distortions on the analytical buckling strength of the aeroshells and to emphasize the importance of accurate modeling by considering real structures for which test data are available.

SYMBOLS

A	cross-sectional area, cm^2
E	modulus of elasticity, GPa
I	area moment of inertia, cm^4
J	torsional constant, cm^4
n	circumferential wave number
p_{cr}	buckling pressure, kPa
R	radius, cm
t	thickness, cm
w_o	amplitude of initial imperfection, cm
$\bar{z}$	normal distance from shell midsurface to stringer centroid, cm
μ	Poisson's ratio

AEROSHELL STRUCTURAL CHARACTERISTICS

The basic aeroshell configuration is a 140^o stiffened cone with a 3.5-meter base diameter and a spherical nose cap. Two structural prototype aeroshells and a flight aeroshell were fabricated for testing; all were fabricated from aluminum. Photographs of two views of one of the structural prototype aeroshells are shown in figure 1. The exterior surface of the shell is shown in the upper photograph. The lower photograph is

of the interior of the shell and shows the nine 40^{o} skin segments, the large base and payload rings, the many small channel-section stiffening rings, and the stringers located in the vicinity of the payload ring. The gross dimensions of the shell are given in figure 2 which shows a cross-sectional schematic view of one-half of the shell. The entire section of the structure (between the 164-cm and 175-cm radii) that forms a closed loop is referred to as the base ring. Detail dimensions of the payload ring and base ring and the locations and proportions of the small channel-section rings are described in appendix A.

A photograph of the interior of the flight aeroshell is shown in figure 3. This shell has a deeper payload ring than the structural prototype and the cone is fabricated from three 120^{o} skin segments. All the small stiffening rings are Z-sections, except for a T-section ring at the nose cap-cone juncture. Figure 4 shows a schematic cross-sectional view of one-half of the shell. The flight aeroshell does not have stringers for local stiffening in the neighborhood of the payload ring as does the prototype aeroshell. Instead, the skin consists of a series of stepped lands, each of a different uniform thickness as shown in the "detail view" insert in figure 4. The closed loop between the 167-cm and the 174-cm radii is referred to as the base ring. Detail dimensions of the payload ring and the base ring, and the locations and the proportions of the Z- and T-rings are given in appendix A. The aeroshells were loaded by uniform external pressure reacted at the payload ring. Details of the loading and the test setup are given in appendix B.

ANALYSIS

Computer Program

Three options of the Structures Research Associates (SRA) system of shell-of-revolution computer programs (refs. 7 and 8), which use forward integration solution techniques, were used for this study. They are: (1) SRA 200 for nonlinear, axisymmetric stress analysis; (2) SRA 201 for bifurcation buckling analysis from a nonlinear, axisymmetric stress state; and (3) SRA 202 for imperfection-sensitivity analysis which assumes a small initial imperfection proportional to the buckling mode shape. The imperfection-sensitivity analytical formulation is based on the method of Koiter (ref. 9) and is presented in detail in reference 10.

The advanced analysis capability of these programs is such that it is now practical to analyze shells with many branches, a feature not available during the design stages of the aeroshells. In addition, these programs have the capability of analyzing general, segmented, meridional shapes with discrete rings, variable material properties and wall cross sections, "smeared" stringers, and arbitrary loads. All results that are presented

for branched-shell models are based on a nonlinear, prebuckling state of stress from a live pressure loading.

Analytical Models

The analytical models of the aeroshells are shown in figure 5. The circle symbols represent the structure modeled as discrete rings. It was not possible to model all the components of the structure as shell branches because the computer code used in the analysis is an in-core program and such modeling would lead to excessive storage requirements. Thus, ring theory was used where it was judged to be adequate, such as for the outstanding flanges of the channels and Z-rings, and (on the prototype) for the entire ring cross section of six of the channel rings in the vicinity of the payload ring where there were longitudinal stiffeners. Discrete rings were also used at joints to reflect more accurately the eccentric load paths. For example, portions of the structure (beyond the rivet lines), which essentially would have zero meridional stress but still provide circumferential stiffness, were also modeled as discrete rings. The structure modeled in this manner is shown as open areas, and the structure actually modeled as a shell is shown shaded or by a single line.

A uniform pressure loading was applied to all models. Since the outstanding edge of the payload ring for each of the aeroshells tested was attached to a rigid test fixture, this edge of the payload ring was assumed to be simply supported for all cases.

Structural prototype aeroshell.- The analytical models of the two structural prototype aeroshells are shown in figure 5(a). The only significant difference in the two prototypes was in the base-ring stiffness. The philosophy behind the base-ring design is discussed in reference 4. Briefly, the base ring was designed to provide the equivalent of simple support at the base of the shell. One shell was designed with a marginally stiff base ring having a mass of 16 kg, and the other shell was designed with a conservatively stiff base ring having a mass of 27 kg. There was also a slight difference in the payload rings for each specimen because of the differences in the method of fabrication; however, both payload rings were structurally equivalent.

The sensitivity of the results to the flexibility of the attachment area of the channel rings was examined by analyzing three different models of each prototype aeroshell. For each aeroshell model, all the channel rings were modeled as one of the three configurations shown in the inset labeled "Ring modeling details" in figure 5(a). Model 2P is judged to be the best representation because it includes the flexibility of the bend radius and the attachment is at the edge of the flange faying surface which, in the actual structure, was bonded, as well as riveted, to the aeroshell skin. In model 1P, the stiffest model, the web is attached directly to the skin; whereas, in model 3P the attachment is considered to be at the rivet line, which clearly permits greater flexibility than is allowed in the actual structure because the bonding is neglected.

Flight aeroshell.- The models of the flight aeroshell are shown in figure 5(b). The sensitivity of the results to the flexibility of the attachment area of the Z-rings was examined by analyzing two different structural models. For each aeroshell model, all the Z-rings were modeled as one of the two configurations shown in the inset labeled "Ring modeling details." Since the attachment flanges of the Z-rings were welded to the skin, they were considered to be attached at the edge of the spot welds. (Bonding was not used in the flight aeroshell.) To conserve computer storage, part of the attachment flange was modeled with classical ring theory, and part, as a branched shell. The area in the bend radius and the area in the flat part of the attachment flange up to the edge of the spot weld were modeled as a single, straight-segment branch of equal area. The remainder of the attachment flange was modeled as a ring. This model is referred to as model 2F. Calculations were also made for the less flexible case of the web directly attached to the shell (model 1F). Model 2F is judged to be the best representation since it approximates a flexibility that is present in the real structure.

RESULTS

This section first presents the buckling-load predictions for all of the branched-shell models studied and compares the results with previous results based on classical ring theory models. Predictions for the buckling loads and mode shapes for the best branched-shell models are then compared with the experimental results. Finally, the sensitivity of the aeroshells to small initial imperfections proportional to the shape of the buckling mode is examined.

Analytical Buckling Loads

Structural prototype aeroshells.- The effects on the analytical buckling pressure of the three model variations are shown by the bar graph in figure 6(a). A comparison of the branched-shell results with the results of reference 4, which are based on the classical ring theory modeling of all rings, shows more than a 30-percent reduction in strength predictions for all three model variations. The results for models 1P and 2P were obtained from the 16-kg base-ring aeroshell and the results for model 3P are from the 27-kg base-ring aeroshell. However, the base rings for both aeroshells were adequate in stiffness to provide the equivalent of simple support during buckling so that both aeroshells exhibited similar buckling behavior. Model 3P is the weakest, as expected. However, as discussed in the previous section, this model is probably not as representative of the real structure as is model 2P. Although model 2P was presumed to be the most representative model of the three, the difference in buckling strength from that calculated for model 1P is small.

Flight aeroshell.- A similar bar graph is shown for the flight aeroshell in figure 6(b). The branched-shell results are compared with a reference model which had the payload and base rings modeled as shell branches, but all other rings were modeled with the classical ring theory. A reduction in strength of more than 55 percent from the reference model is shown. Even though model 2F is considered to be the more realistic representation of the actual structure, model 1F shows that modeling the Z-ring webs as shell branches accounts for most of the discrepancy between the branched shell and the ring theory analysis. Although the strength predictions for the branched-aeroshell models show a drastic reduction from the classical ring theory predictions, it does not necessarily follow that a large increase in mass would be required to meet design conditions. For example, in reference 3, design studies of similar shells show that only about a 4-percent increase in mass would be required if a branched-shell analysis were used instead of ring theory in the design process.

Comparison of Theory and Experiment

Structural prototype aeroshells.- Buckling pressure is shown as a function of circumferential wave number n in figure 7(a) for the 16-kg base-ring aeroshell and in figure 7(b) for the 27-kg base-ring aeroshell. The solid curves are for branched-shell model 2P and pass through a minimum at $n = 7$. The dashed curves labeled "Ring theory" represent buckling results for rings modeled with the classical ring theory and, along with the test data, are taken from reference 4. The dashed curves overestimate the experimental buckling strength by about 40 percent and do not predict the observed buckling mode. However, the solid curves for the refined (branched-shell) models accurately predict both the failure loads and the circumferential buckle patterns observed in the tests.

Flight aeroshell.- Figure 7(c) shows the corresponding results for the flight aeroshell. The dashed curve labeled "Ring theory" in this figure, however, is for the structure modeled with a branched payload ring and a branched base ring; for all other rings the classical ring theory is used. As can be seen, the test result falls far below the minimum point on the dashed curve ($n = 5$) which overestimates the buckling pressure by 250 percent. A remodeling of the structure so that all the rings are allowed to deform by treating them as a shell (model 2F) brings the theory (solid curve) into much better agreement with the test point. The theory curve is also brought well within the bounds of the 0.8 knockdown factor established from tests of similar stiffened cones reported in the literature. The minimum point on the solid curve occurs at $n = 7$; however, the shell was observed to buckle into six circumferential waves.

Meridional Buckling Mode Shapes

The meridional buckling mode shapes for the 16-kg base-ring prototype aeroshell and the flight aeroshell are shown in figures 8(a) and 8(b), respectively. The mode shape for the 27-kg base-ring prototype aeroshell is omitted since there is no discernible difference from the 16-kg base-ring aeroshell. The dashed lines represent the undeformed profiles and the solid lines represent the deformed profiles. Even though the deformations have been amplified for plotting purposes, it is clear that, for both aeroshells, considerable distortion of the ring sections has occurred at the buckling load. The Z-rings of the flight aeroshell were of thinner gage material than the channel rings of the prototype and show an even greater deformation at the buckling load.

Comparison With Stiffened Flat-Plate Data

The rather large discrepancies that exist between the ring-theory predictions (see dashed curve, fig. 7(a), for example) and the test data are in contrast to experience based on results from flat plates loaded in compression. For example, in reference 11 flat panels with essentially identical proportions to the aeroshell stiffened wall and having a length equal to half the circumferential buckling wave length were shown to be well-behaved. The critical buckling stress was nearly three times as great as the average stress at buckling for the prototype wall section. Thus, it would appear that the prototype aeroshell-buckling behavior is not a simple function of wall cross section, but is a rather complicated function of the geometry and loading. Such behavior requires an analysis that accounts for detail behavior of the ring stiffeners for accurate predictions.

Imperfection-Sensitivity Analysis

Initial imperfections in the structural prototype and flight aeroshells were measured to some extent prior to testing, and the results for the flight aeroshell are presented in reference 3. The largest measured imperfection for the prototype aeroshell was about three times the skin thickness, and for the flight aeroshell, the largest measured imperfection was slightly more than two thicknesses. In order to study the sensitivity of the aeroshells to initial imperfections having the shape of the buckling mode, models 2P and 2F were analyzed. The results are presented in figure 9 where buckling pressure p_{cr} is plotted as a function of the ratio of imperfection amplitude to skin thickness w_o/t.

Structural prototype aeroshells.- Three buckling modes for each of the prototype aeroshells were examined and the results are shown in figure 9(a) for the 16-kg base-ring aeroshell and in figure 9(b) for the 27-kg base-ring aeroshell. The sensitivity of the critical mode, $n = 7$, is shown by the solid lines; the broken lines are for the two neighboring buckling modes. The $n = 7$ mode remains critical over the range of

imperfection amplitudes examined (up to twice the skin thickness); at the maximum imperfection shown, a 20-percent reduction in strength from the perfect-shell value is predicted. The $n = 6$ and $n = 8$ buckling modes exhibit similar behavior.

It should be recognized that the theory for the imperfect shells falls below the test values. Such behavior may indicate that the type of imperfection studied herein was not present in the fabricated shells. However, the theoretical results are based on nominal skin gage since the test articles have not yet been sectioned in order to make accurate skin-gage measurements. One of the most difficult details to model accurately was that of the stringers, because their properties must be distributed uniformly and they contained many cutouts in order to accommodate the rings. The assumptions were considered to be conservative so that the stiffener effectiveness is probably greater than is represented in the analysis.

Flight aeroshell.- Corresponding studies were made for the flight aeroshell and the results are presented in figure 9(c). It is immediately obvious that this shell is practically insensitive to initial imperfections of the type examined, none of the modes showing more than a 5-percent reduction from perfect-shell results. Thus, it appears that initial imperfections in the external shell are probably not responsible for the difference between branched-shell theory and the test results shown in figure 7(c). An interesting aspect of the curves in figure 9(c) is the crossing over of the $n = 6$ and $n = 7$ curves so that the $n = 6$ mode (the observed number of buckling waves in the failed aeroshell) becomes critical for the imperfect shell.

CONCLUDING REMARKS

One of the most advanced shell-of-revolution computer programs available has been used to analyze highly refined structural models of three blunt, conical shells which approached optimum design proportions. The shells were stiffened with many thin-gage, open-section rings and exhibited behavior in contrast with previous buckling-test data. Conventional analysis in which the ring sections are assumed to be rigid is shown to be highly unconservative for the shells studied. The application of a knockdown factor (established from earlier tests of blunt conical shells stiffened with many closed-section rings) on the general instability could not bring the theory and test data into agreement. A more refined, branched-shell analysis shows that thin-gage, open-section rings attached to blunt cones are susceptible to shell-type distortion and do not necessarily behave as stiffeners of similar proportions attached to flat plates. The refined analysis gave results that were in excellent agreement with experimental results for two of the shells; for the third shell, the results were well within the bounds of the 0.8 knockdown factor reported in the literature for ring-stiffened, blunt cones. Thus, the advanced shell-of-revolution computer programs can accurately predict structural

behavior of these complex shell structures and can provide a powerful tool for a better understanding of such structures.

The buckling loads for the refined models of the aeroshells showed little sensitivity to an initial imperfection proportional to the buckling-mode shape. However, for the one case where perfect-shell theory did not predict the observed buckling mode shape, the inclusion of an initial imperfection brought theoretical results into agreement with test results. The results of the imperfection-sensitivity analysis indicate that accuracy in modeling of the structure is crucial and, unless the model is representative of the real structure, initial imperfections may erroneously be blamed for inaccurate predictions.

The results of this study show that there is a need for additional research in the area of buckling of stiffened shells. Although it is obvious to conclude that an accurate analysis of realistic structural models leads to accurate predictions, it is important to know when such analyses are required since they may become expensive and complicated for complex structures. Ring proportions and spacings on shells of all types should be studied to determine when rings can be modeled simply as rings and when a branched-shell analysis should be applied.

Langley Research Center,
National Aeronautics and Space Administration,
Hampton, Va., November 21, 1974.

APPENDIX A

DETAIL DIMENSIONS OF AEROSHELLS

Structural Prototype Aeroshells

Two structural prototype aeroshells were fabricated. The only significant structural difference in the two was in the payload-ring and base-ring configurations. The detail dimensions of the two payload rings are given in figure 10, and the two base rings are dimensioned in figure 11. The proportions and locations of the small channel-section rings are given in figure 12. For reference purposes, these rings are numbered consecutive from 1 to 35, starting with the ring on the spherical cap. (See fig. 2.) Although these rings are variably spaced throughout the shell, there are only three different cross-sectional proportions. In addition to the rings, there are 36 equally spaced stringers attached to the shell in the vicinity of the payload ring. The stringer material and mechanical properties used for the analytical model and their location on the shell are given in table I. All the components of the structural prototype aeroshells were joined by riveting; however, adhesive bonding was used in addition to the rivets in an attempt to retard local buckling of the skin between the rivets.

Flight Aeroshell

The detail dimensions of the payload and base rings for the flight aeroshell are given in figure 13. The payload-ring web was stiffened with 40 equally spaced stringers whose properties were uniformly distributed around the circumference. The material and mechanical properties of the stringers used for modeling are given in the figure. There are 27 small, variably spaced Z-rings and, for reference purposes, they are numbered sequentially from 1 to 27, starting with the Z-ring nearest the nose cap-cone juncture. (See fig. 4.) All these rings have identical thicknesses with the exception of ring number 10. Proportions and locations of the Z-rings and the T-ring are given in figure 14.

APPENDIX B

TEST SETUP AND LOADING CONDITIONS

Structural Prototype

A schematic representation of the test setup for the prototype aeroshells is shown in figure 15. The test specimen was continuously supported at the outstanding flange of the payload ring on a machined surface of the test fixture. The test fixture and the aeroshell formed a vacuum chamber with the exterior surface of the aeroshell exposed to atmospheric pressure. A uniform external-pressure loading on the aeroshell was attained by evacuating the chamber. The membrane pressure seal between the base ring and the test fixture was designed to produce a minimal load on the base ring during loading.

Flight Aeroshell

The flight aeroshell test setup is shown in figure 16. The loading was basically the same as for the prototype, with uniform pressure reacted at the payload ring. For tests of the flight aeroshell under realistic loads, however, hydraulic jacks were used to provide the effect of inertial relief loading at three points of concentrated mass on the aeroshell (tanks and propulsion module) and at six points on the lander body. The lander body was installed on the payload ring during tests in order to simulate a proper load introduction between the aeroshell and the lander.

REFERENCES

1. Bushnell, David: Evaluation of Various Analytical Models for Buckling and Vibration of Stiffened Shells. AIAA J., vol. 11, no. 9, Sept. 1973, pp. 1283-1291.

2. Martin, James S Jr.; and Soffen, Gerald A.: The Viking Mission. Volume 31 of AAS Science and Technology Series, Saul Ferdman, ed., Univelt, Inc., 1973, pp. 127-164.

3. Leonard, Robert W.; Anderson, Melvin S.; and Heard, Walter L., Jr.: Design of a Mars Entry "Aeroshell." NASA paper presented at International Symposium on Buckling of Structures (Cambridge, Mass.), June 1974.

4. Heard, Walter L., Jr.; Anderson, Melvin S.; Anderson, James Kent; and Card, Michael F.: Design, Analysis, and Tests of a Structural Prototype Viking Aeroshell. J. Spacecraft & Rockets, vol. 10, no. 1, Jan. 1973, pp. 56-65.

5. Anderson, James Kent; and Davis, Randall C.: Buckling Tests of Two 4.6-Meter-Diameter, Magnesium Ring-Stiffened Conical Shells Loaded Under External Pressure. NASA TN D-7303, 1973.

6. Anon.: Buckling of Thin-Walled Truncated Cones. NASA SP-8019, 1968.

7. Cohen, Gerald A.: Computer Analysis of Ring-Stiffened Shells of Revolution. NASA CR-2085, 1973.

8. Cohen, Gerald A.: User Document for Computer Programs for Ring-Stiffened Shells of Revolution. NASA CR-2086, 1973.

9. Koiter, Warner Tjardus: On the Stability of Elastic Equilibrium. NASA TT F-10833, 1967.

10. Cohen, Gerald A.: Computer Program for Analysis of Imperfection Sensitivity of Ring-Stiffened Shells of Revolution. NASA CR-1801, 1971.

11. Hickman, William A.; and Dow, Norris F.: Data on the Compressive Strength of 75S-T6 Aluminum-Alloy Flat Panels Having Small, Thin, Widely Spaced, Longitudinal Extruded Z-Section Stiffeners. NACA TN 1978, 1949.

TABLE I.- STRINGER PROPERTIES FOR STRUCTURAL PROTOTYPE AEROSHELLS

[E = 73.08 GPa; μ = 0.32]

R, cm	A, cm^2	I, cm^4	J, cm^4	$\bar{z}$, cm	Meridional variation	Number of stringers
47.12	0.094	0.00194	0.00013	2.46	Constant	18
52.63	.256	.00452	.00383	2.58	Constant	18
54.43	.256	.00452	.00383	2.58	Constant	36
64.59	.256	.00452	.00383	2.58	Linear taper	36
67.81	.342	.00824	.00235	2.50	Linear taper	36
74.03	.586	.01011	.00443	2.59		
74.03	.749	.01701	.00582	2.64	Linear taper	36
78.44	.889	.03813	.00688	3.32	Constant	36
81.58	.889	.03813	.00688	3.32	Linear taper	36
87.40	.735	.03610	.00557	2.61		
87.40	.572	.02721	.00418	2.55	Linear taper	36
92.96	381	.02281	.00255	2.50		
92.96	.218	.01356	.00117	2.39	Constant	36
95.65	.218	.01356	.00117	2.39	Constant	18
103.21	.113	.00720	.00015	2.36	Constant	18
105.65						

Figure 1.- Photographs of structural prototype aeroshell.

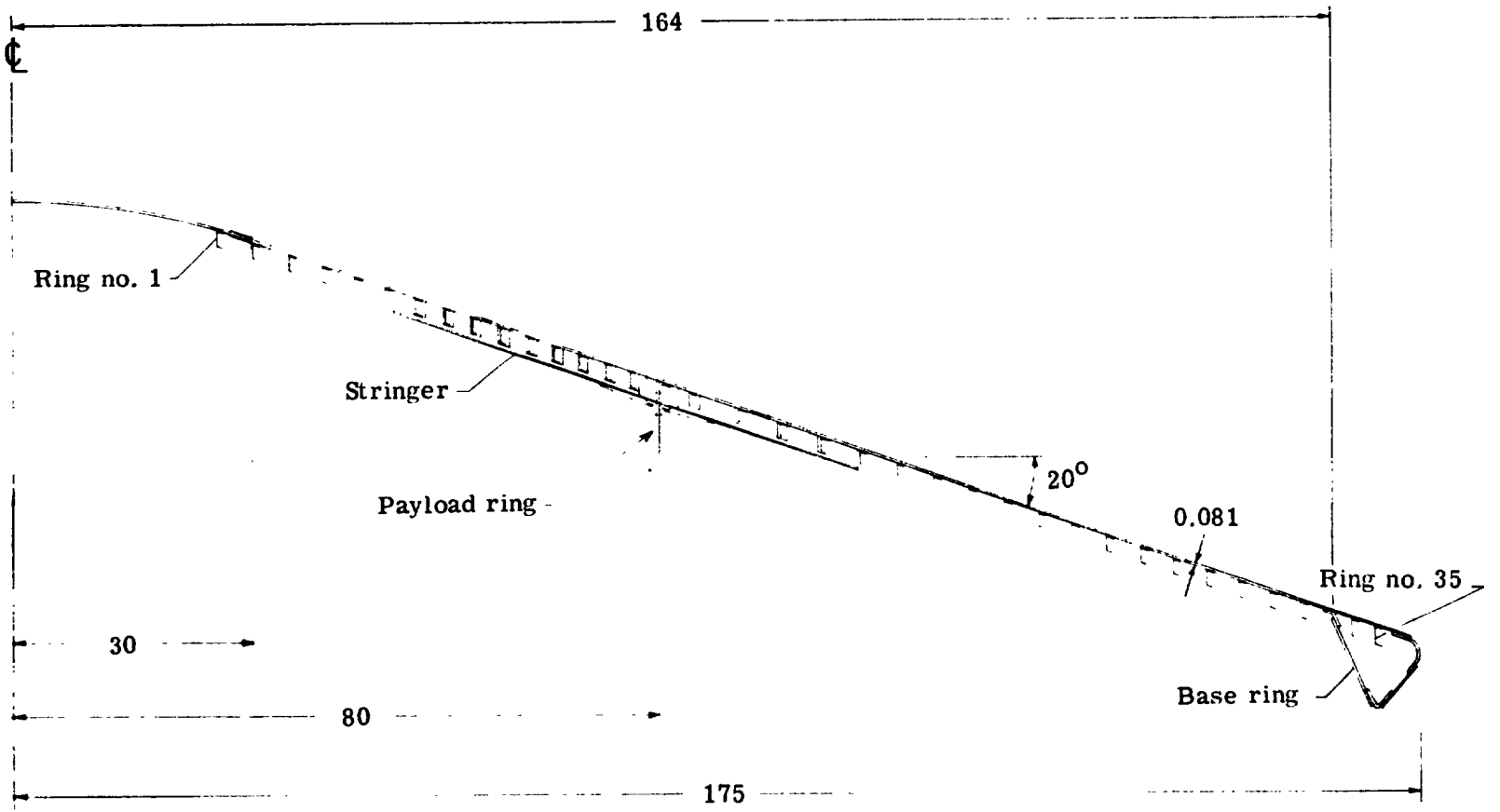

Figure 2.- Cross-sectional schematic view of structural prototype aeroshell. Dimensions are in cm.

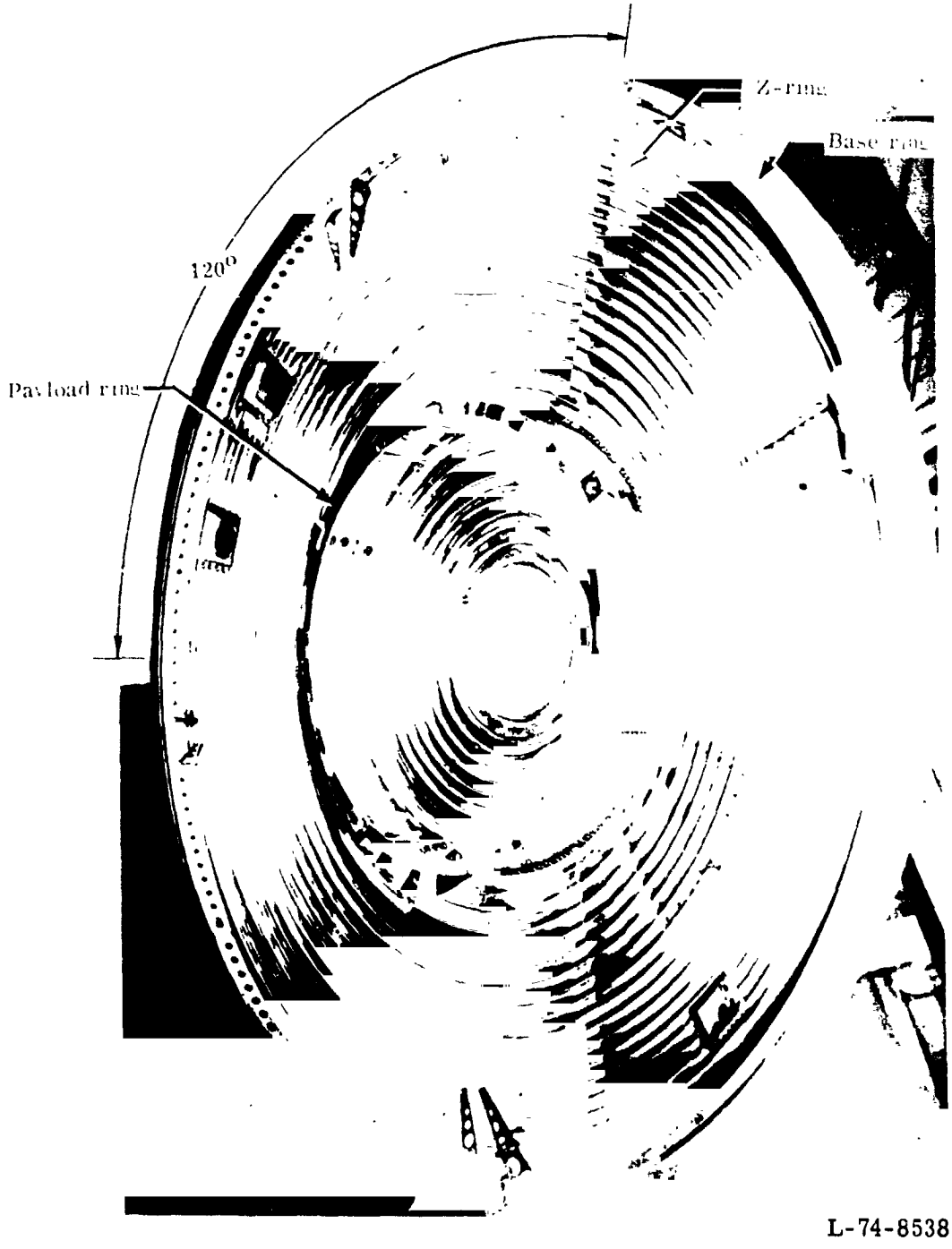

Figure 3.- Flight aeroshell.

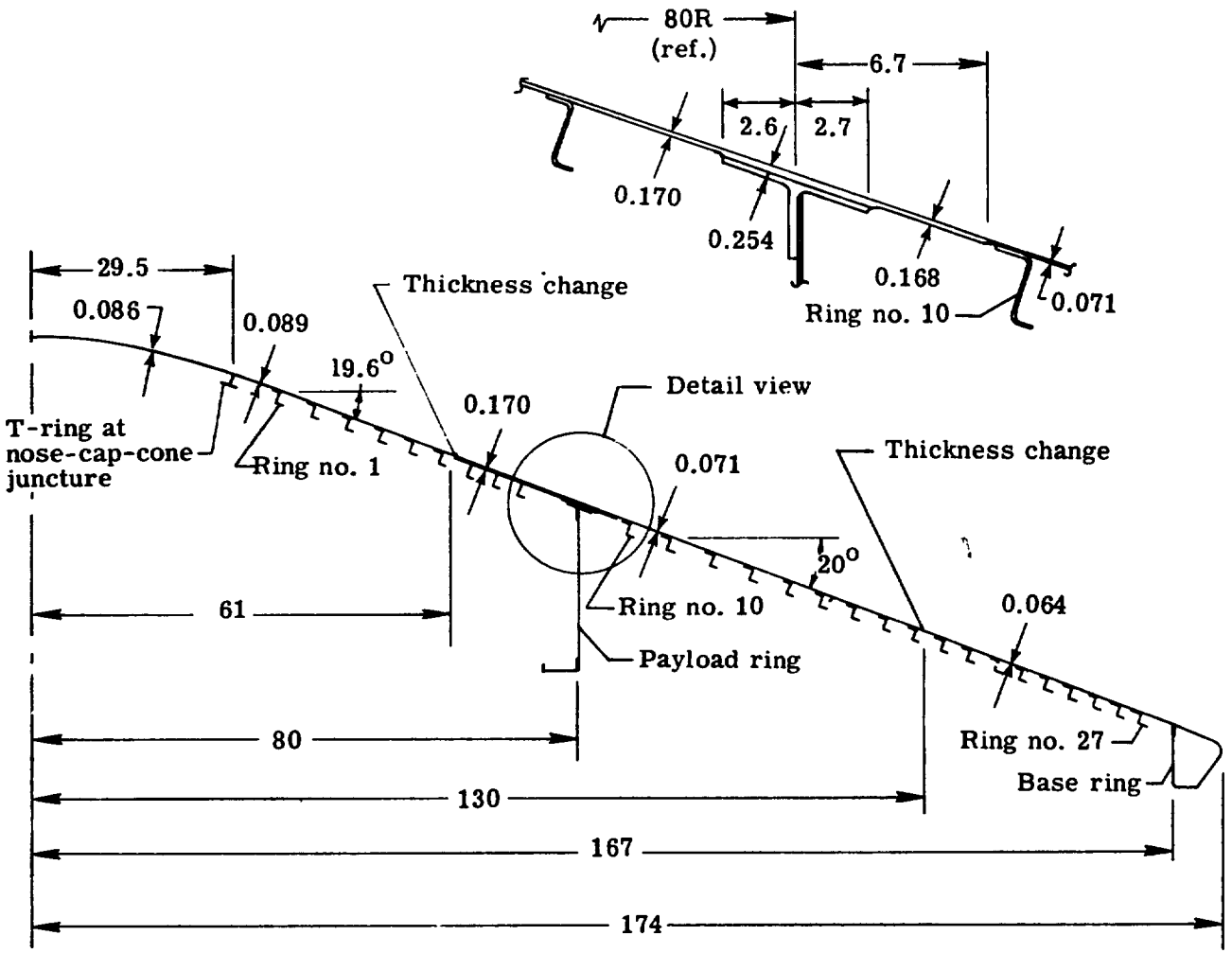

Figure 4.- Cross-sectional view of flight aeroshell. Dimensions are in cm.

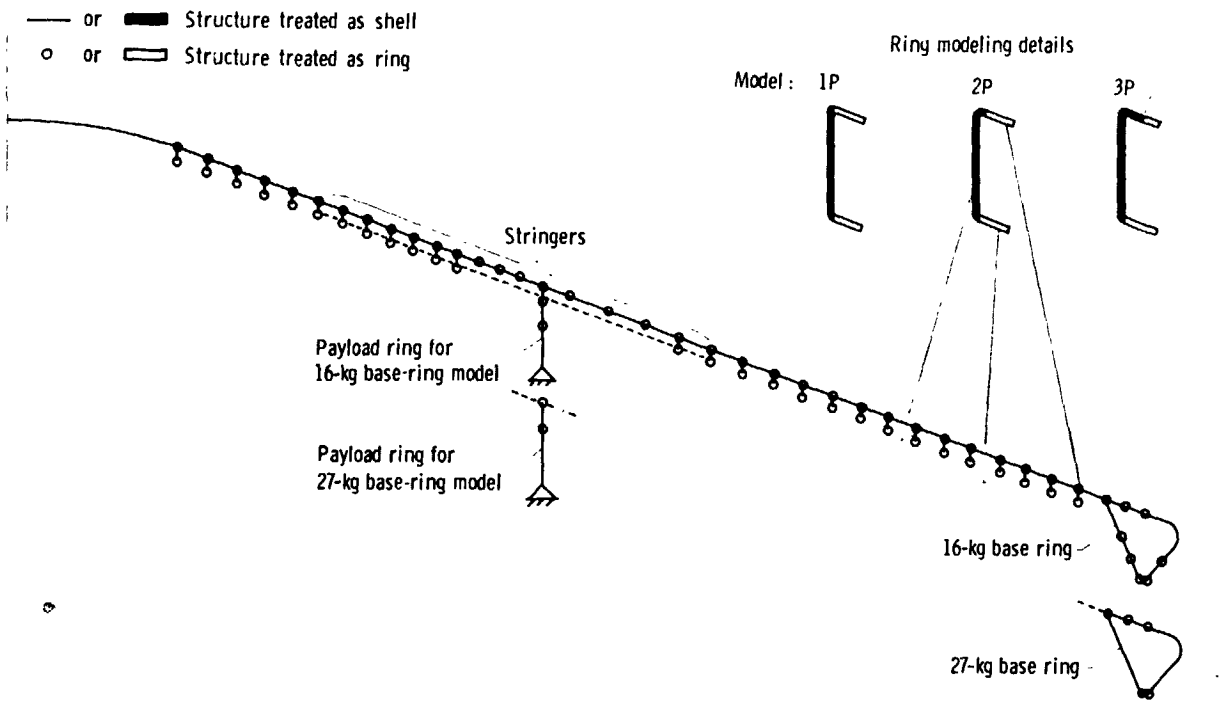

(a) Structural prototype aeroshells.

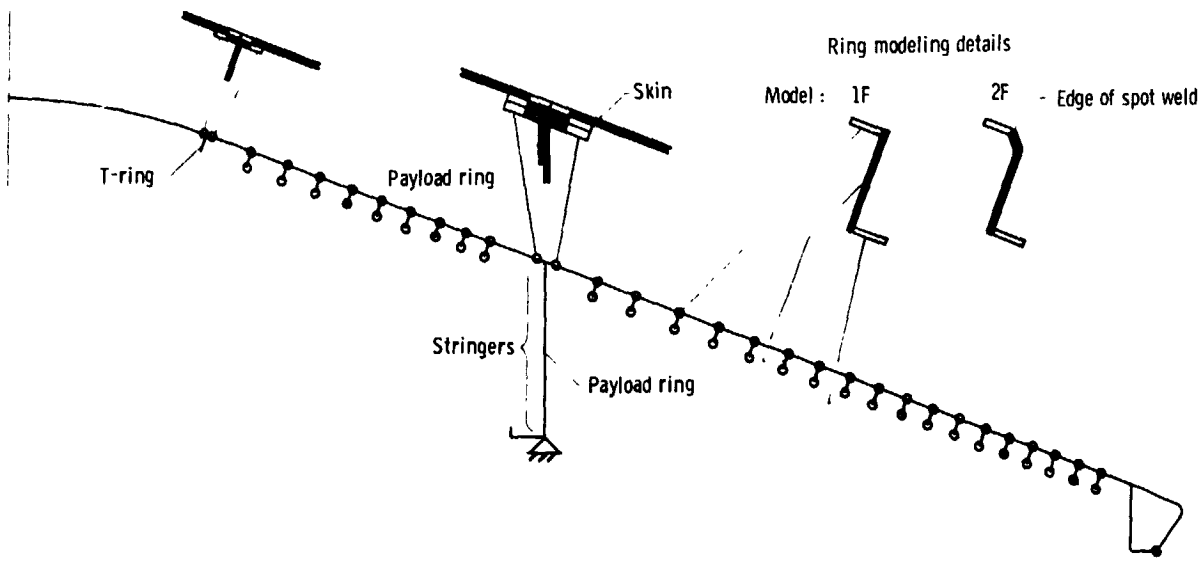

(b) Flight aeroshell.

Figure 5.- Branched-shell analytical models.

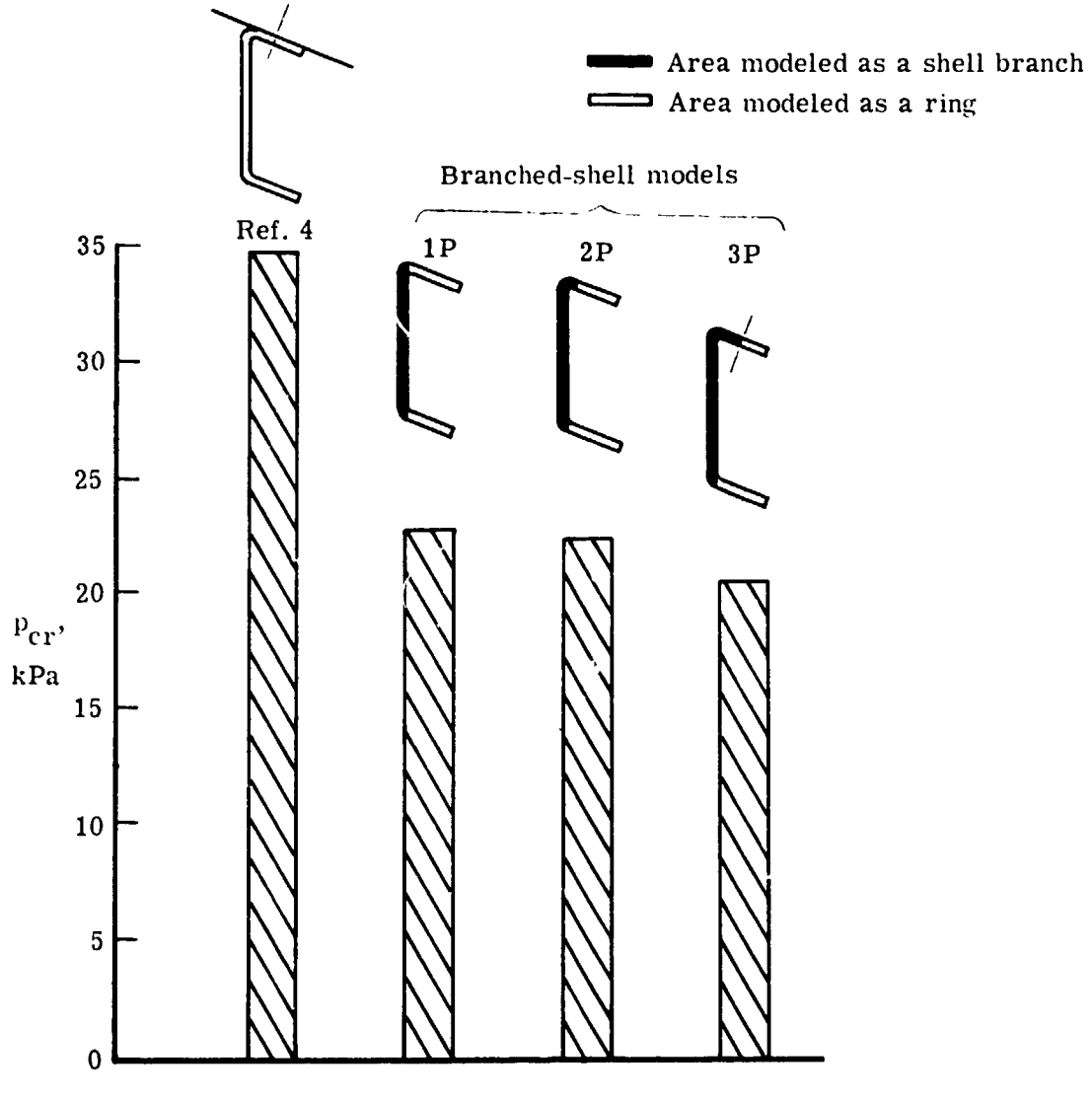

(a) Structural prototype aeroshells.

Figure 6.- Effect of ring-model variations on critical buckling pressure.

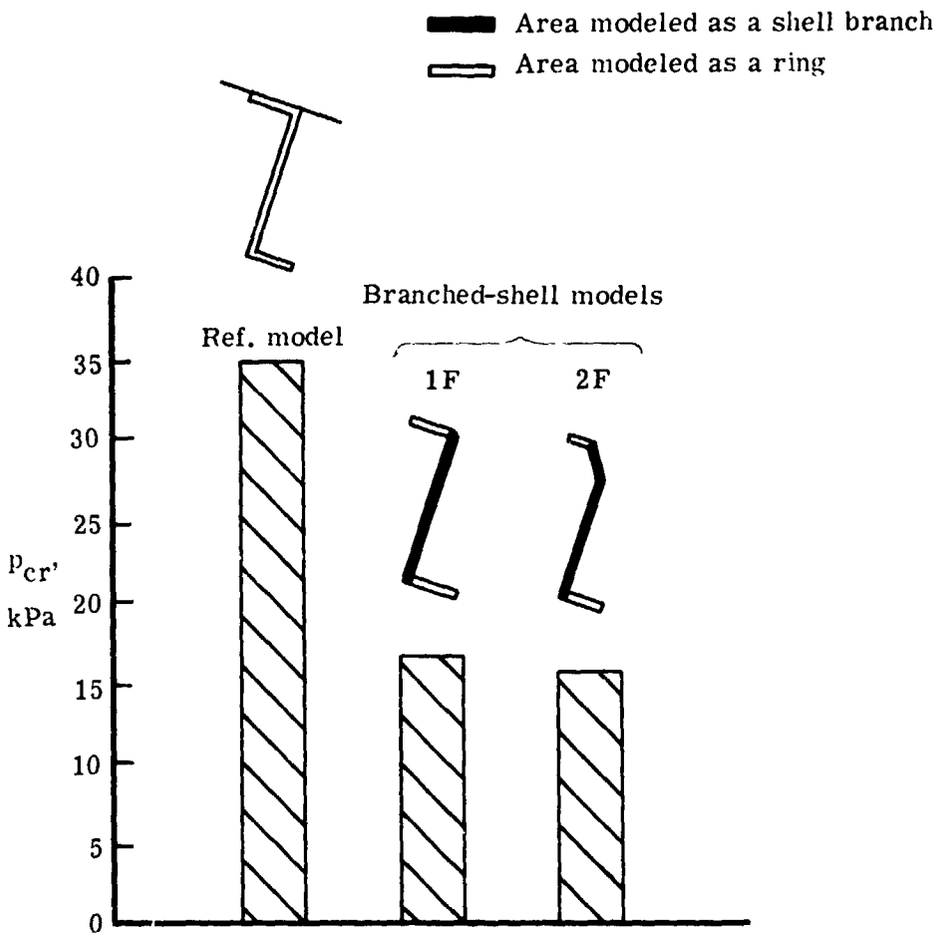

(b) Flight aeroshell.

Figure 6.- Concluded.

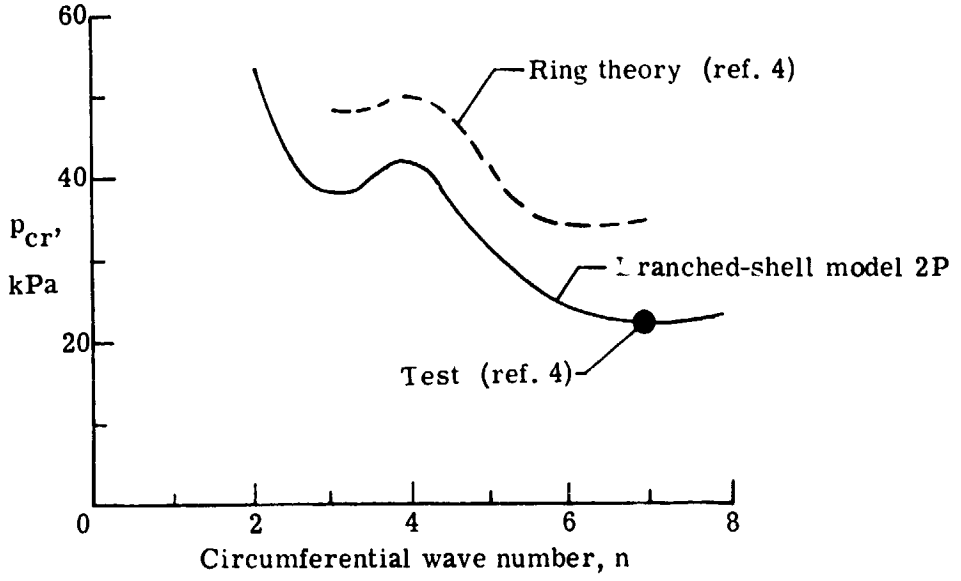

(a) Structural prototype; 16-kg base ring.

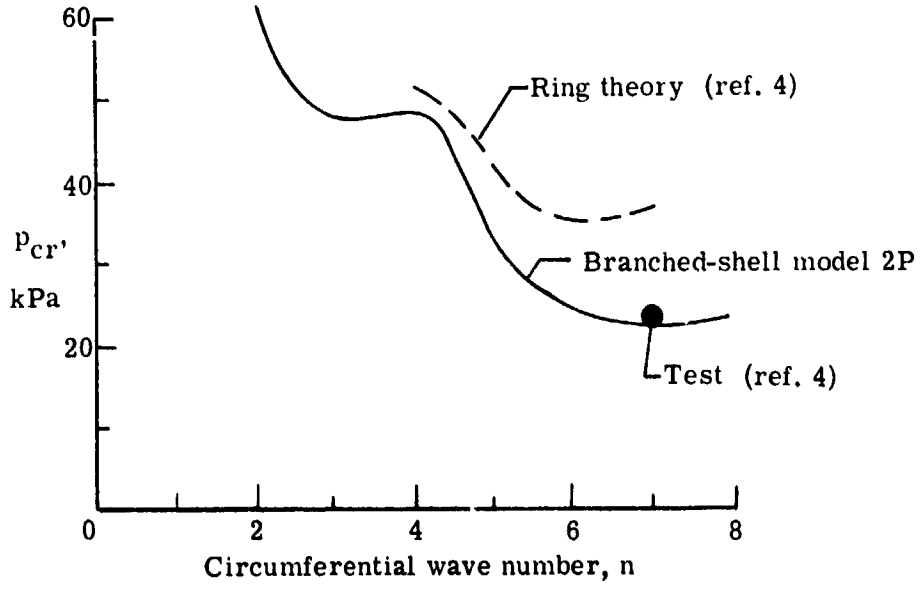

(b) Structural prototype; 27-kg base ring.

Figure 7.- Buckling pressure as a function of circumferential wave number and comparison with experiment.

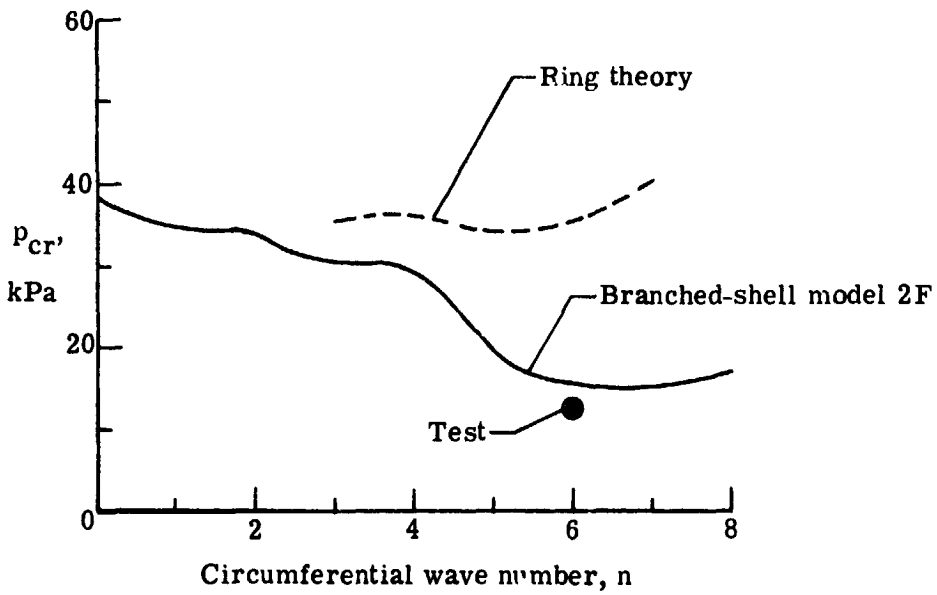

(c) Flight aeroshell.

Figure 7.- Concluded.

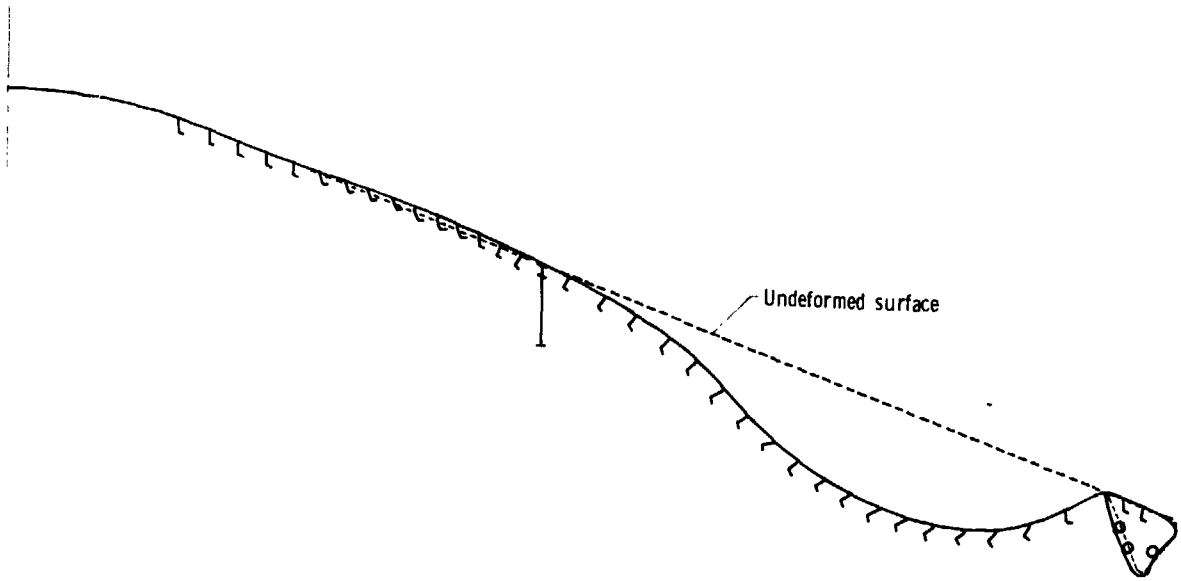

(a) Prototype aeroshell; n = 7.

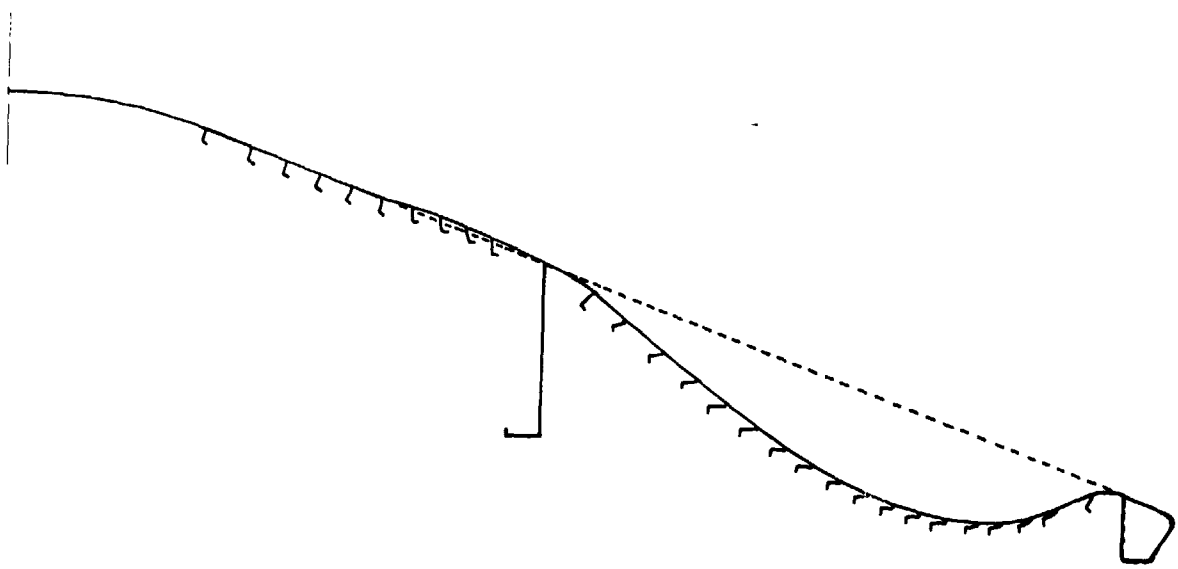

(b) Flight aeroshell; n = 7.

Figure 8.- Meridional buckling mode shapes. Branched-shell calculations.

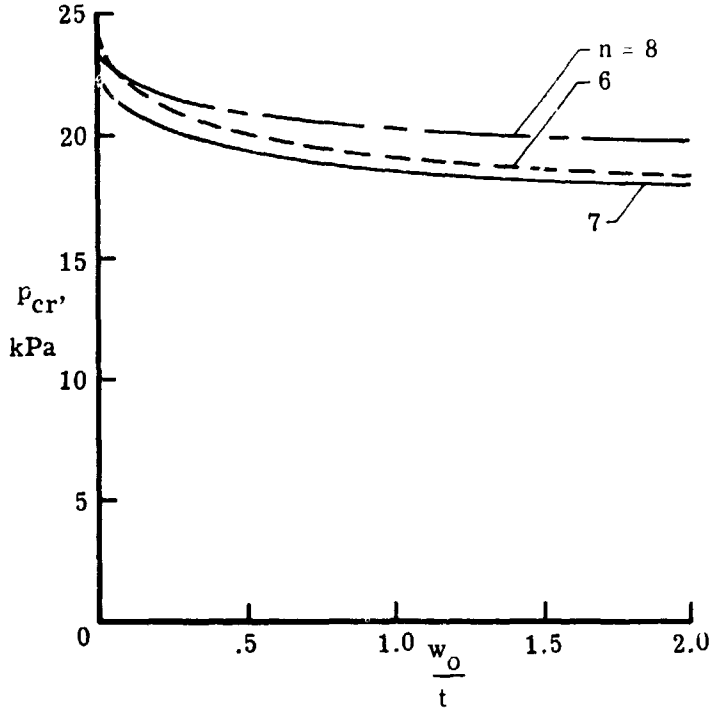

(a) Structural prototype; 16-kg base ring.

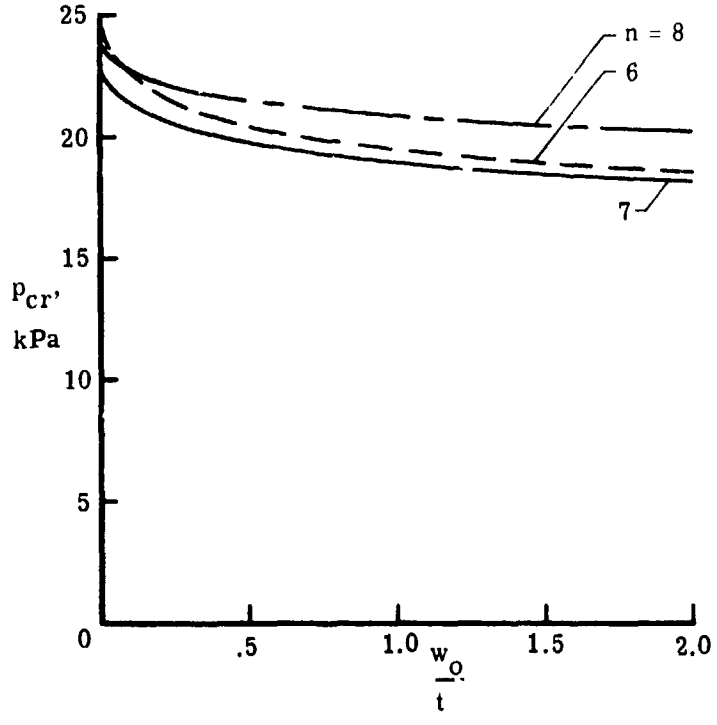

(b) Structural prototype; 27-kg base ring.

Figure 9.- Sensitivity of buckling loads to amplitude of initial imperfection having shape of buckling mode (t = 0.081 cm).

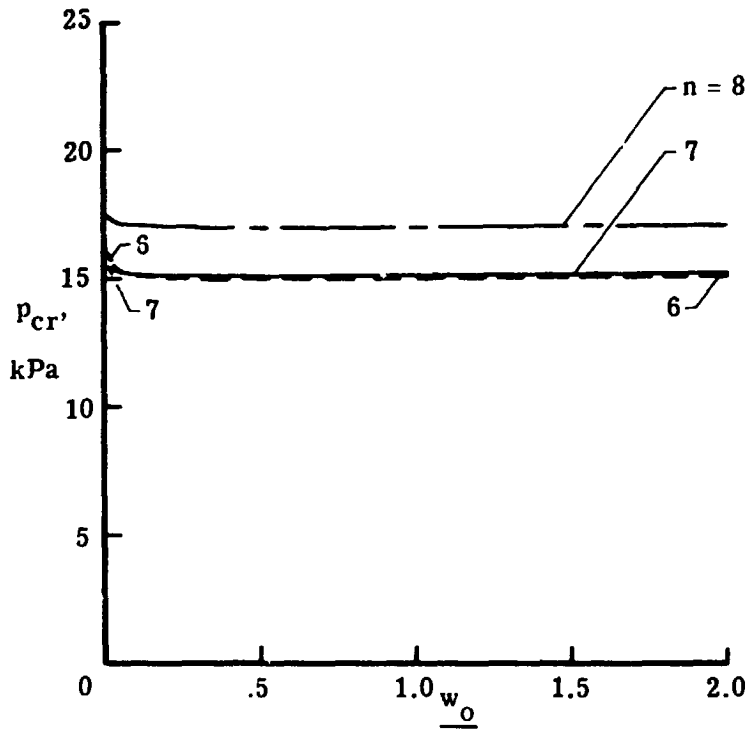

(c) Flight aeroshell (t = 0.061 cm).

Figure 9.- Concluded.

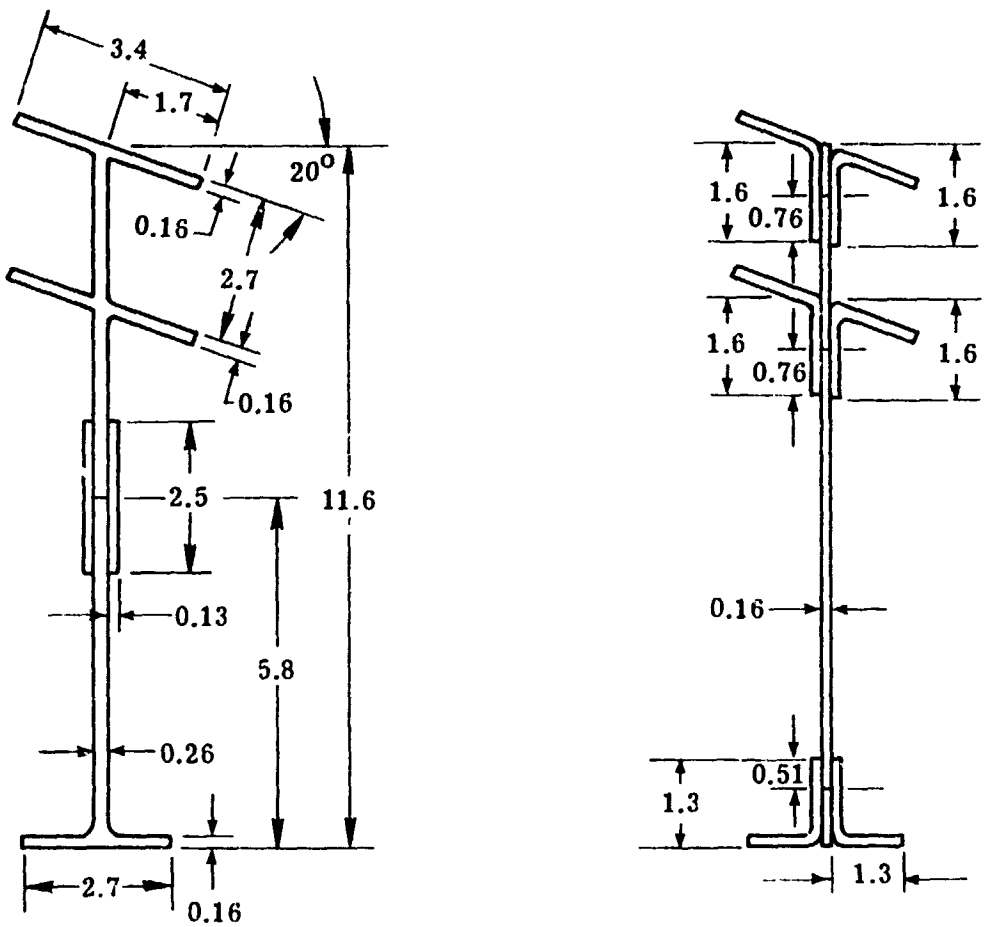

(a) 16-kg base-ring aeroshell. (b) 27-kg base-ring aeroshell.

Figure 10.- Payload ring cross sections for structural prototype aeroshells. Dimensions are in cm.

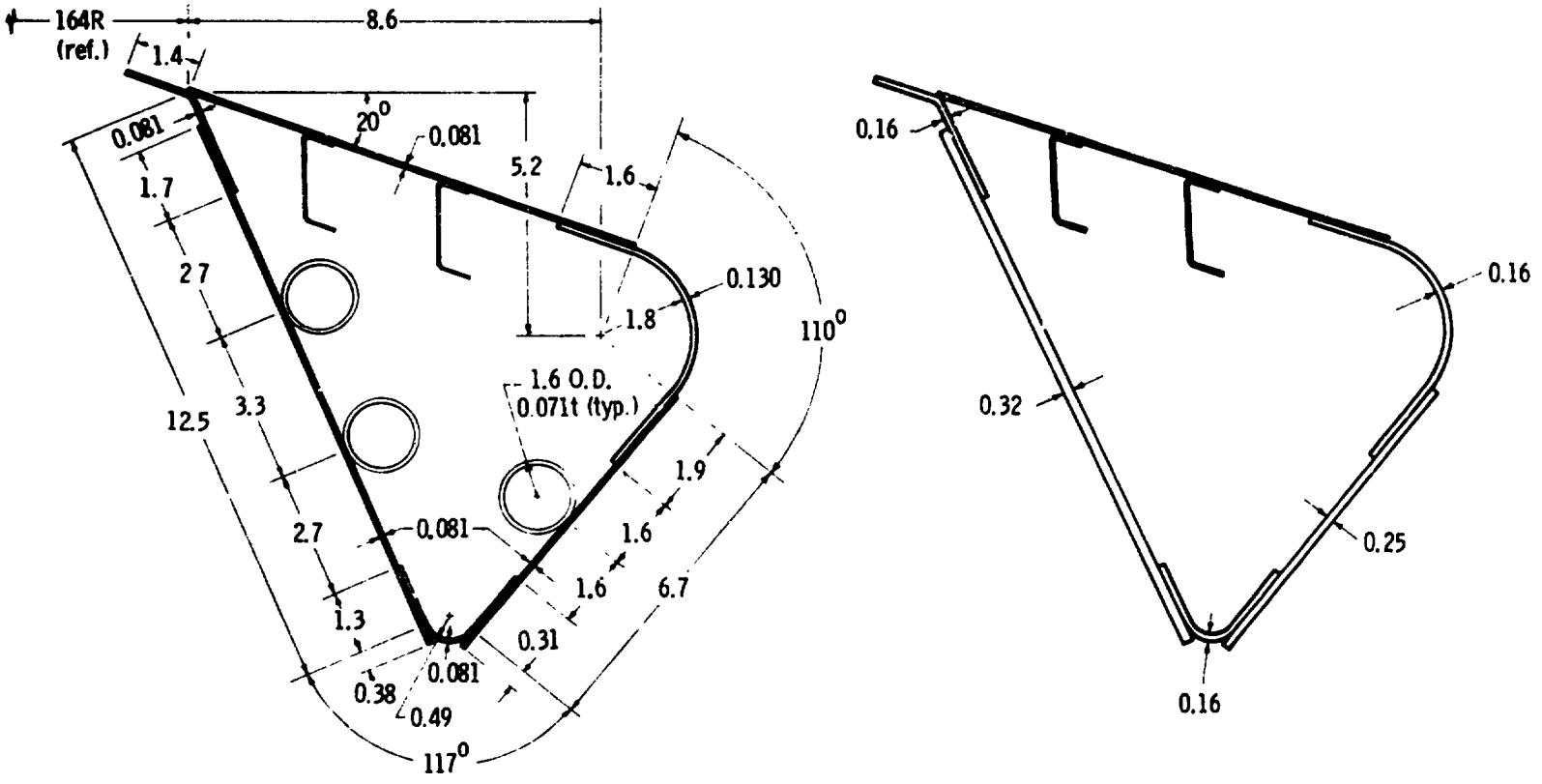

(a) 16-kg base ring.

(b) 27-kg base ring.

Figure 11.- Base-ring cross sections for structural prototype aeroshells. Dimensions are in cm.

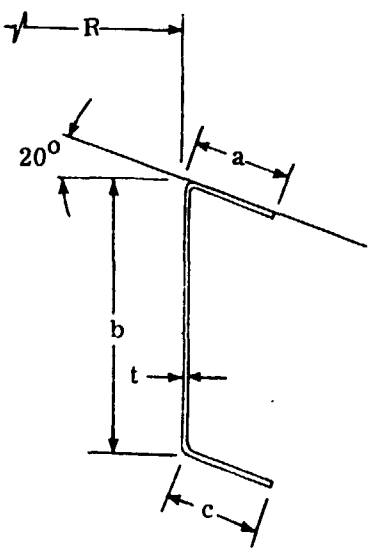

Ring cross section

Ring no.	Dimensions, cm				
	R	a	b	c	t
1	25.70	0.76	2.01	0.81	0.041
2	30.18				
3	34.65				
4	38.89				
5	42.90				
6	46.76				
7	50.50				
8	54.08				
9	57.56				
10	60.93				
11	64.24				
12	67.46				
13	70.59				
14	73.69		↓	↓	↓
15	76.68		2.01	.81	.041
16	84.18		1.68	.69	.051
17	89.92				
18	95.30				
19	100.41				
20	105.28				
21	110.01				
22	114.55				
23	119.00				
24	123.32		↓	↓	↓
25	127.53		1.68	.69	.051
26	131.60		1.96	.79	.064
27	135.86				
28	140.03				
29	144.12				
30	148.16				
31	152.15				
32	156.06				
33	159.92				
34	166.45	↓	↓	↓	↓
35	169.27	.76	1.96	.79	.064

Figure 12.- Ring-stiffener cross sections and locations on structural prototype aeroshells.

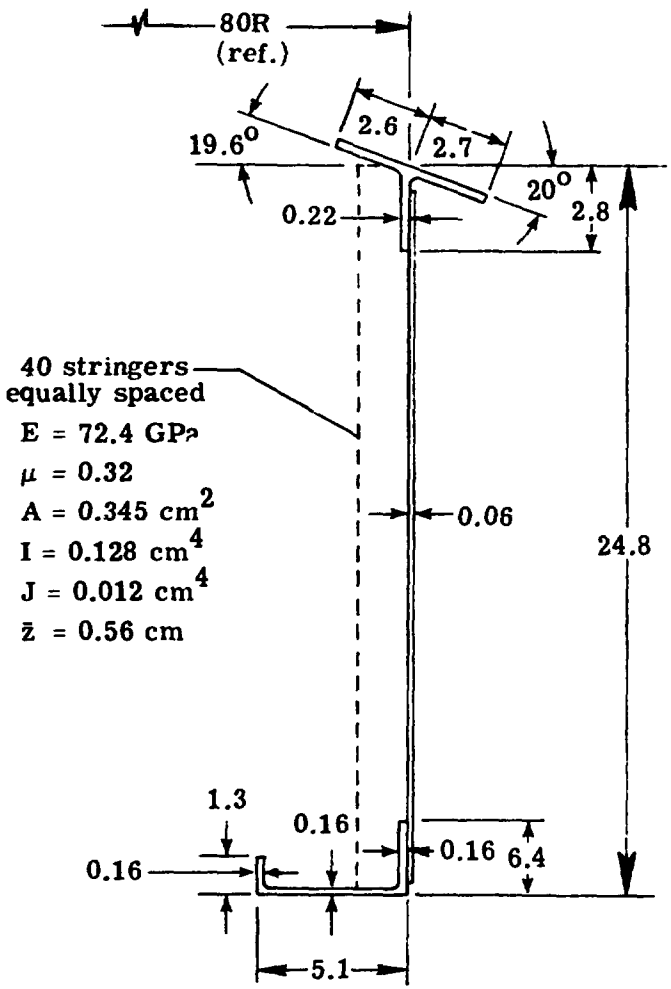

(a) Payload ring.

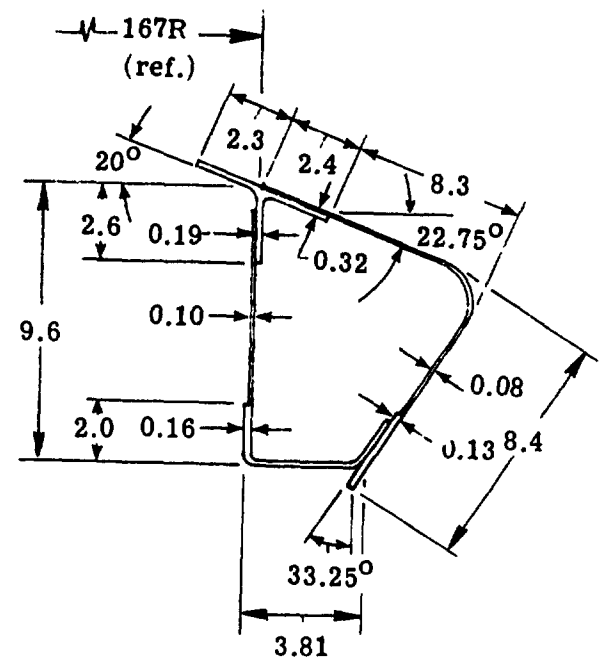

(b) Base ring.

Figure 13.- Components of flight aeroshell. Dimensions are in cm.

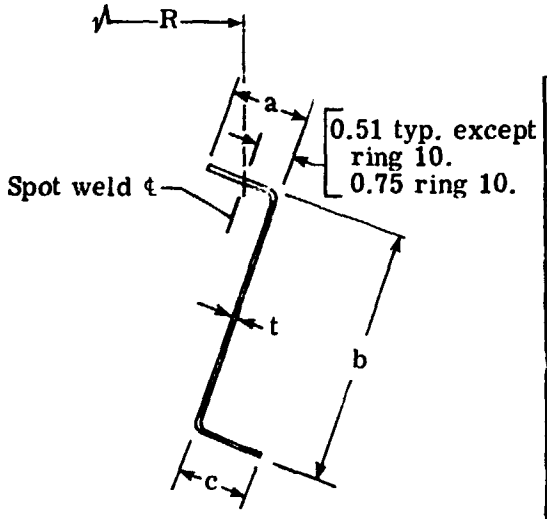

Z-rings

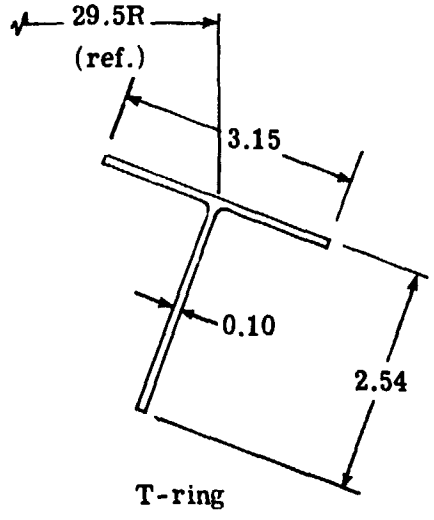

T-ring

Ring no.	Z-ring dimensions, cm				
	R	a	b	c	t
1	34.18	1.02	2.16	0.89	0.041
2	41.42				
3	46.41				
4	51.13				
5	55.68				
6	60.05				
7	64.26				
8	68.05	↓	↓	↓	↓
9	71.70	1.02	2.16	0.89	0.041
10	87.55	1.31	2.44	1.02	.081
11	93.37	1.02			.041
12	99.75				
13	105.51				
14	110.82				
15	115.80				
16	120.50				
17	124.97				
18	129.24				
19	133.35				
20	137.31				
21	141.17				
22	144.91				
23	148.54				
24	152.07				
25	155.52				
26	158.90	↓	↓	↓	↓
27	162.20	1.02	2.44	1.02	.041

Figure 14.- Cross-sectional proportions and locations of rings on flight aeroshell.

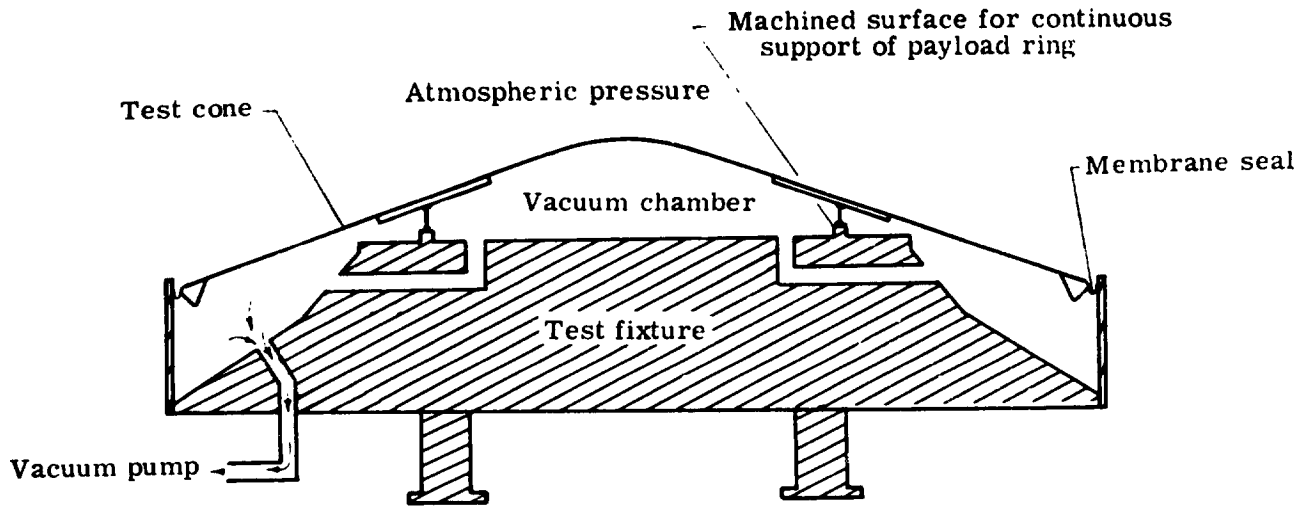

Figure 15.- Schematic representation of test setup showing loading conditions for structural prototype aeroshells.

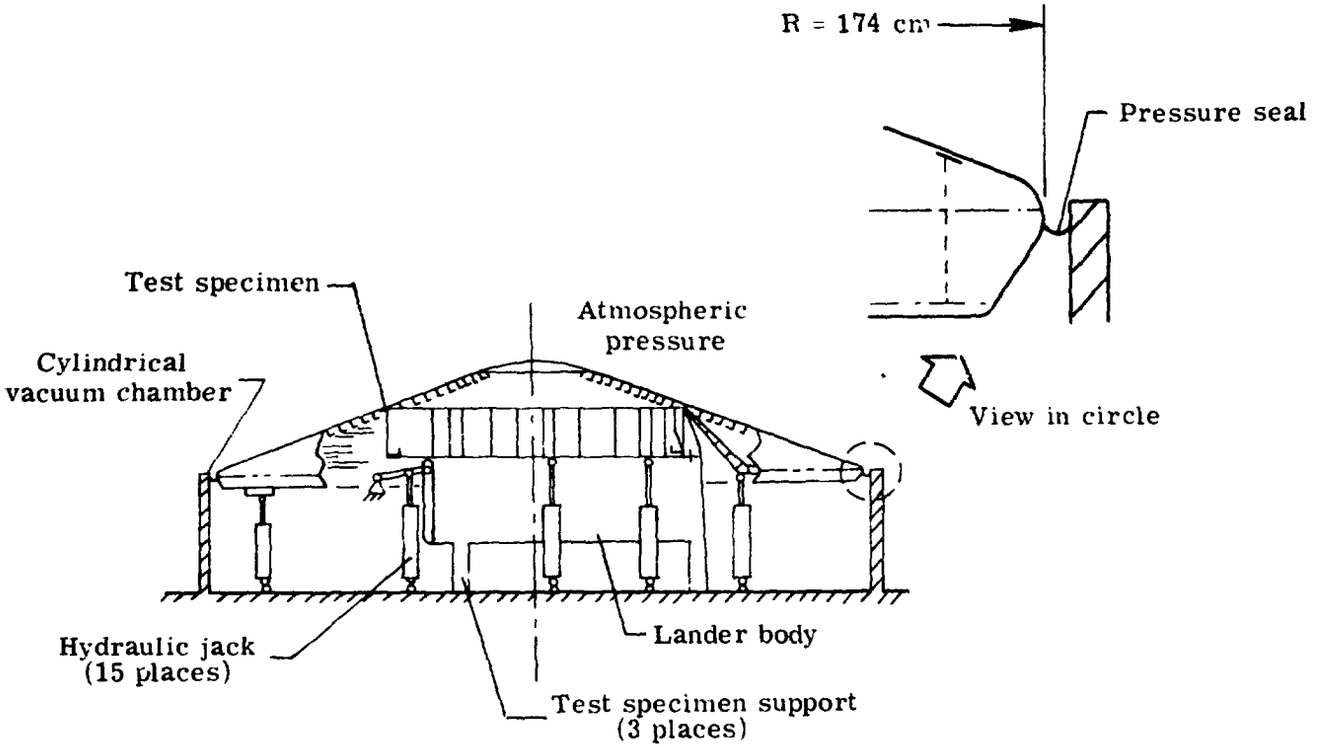

Figure 16.- Schematic representation of test setup showing loading conditions for flight aeroshell.